Contributions to Geophysics and Geodesy Vol. 45/3, 2015 (173–192)

Estimation of the impact of climate change-induced extreme precipitation events on floods

Kamila HLAVČOVÁ[1], Milan LAPIN[2], Peter VALENT[1], Ján SZOLGAY[1], Silvia KOHNOVÁ[1], Peter RONČÁK[1]

[1] Department of Land and Water Resources Management, Slovak University of Technology, Radlinského 11, 810 05 Bratislava, Slovakia, kamila.hlavcova@stuba.sk

[2] Division of Meteorology and Climatology, KAFZM, FMFI, Comenius University, Mlynská dolina, 842 48 Bratislava, Slovakia

Abstract: In order to estimate possible changes in the flood regime in the mountainous regions of Slovakia, a simple physically-based concept for climate change-induced changes in extreme 5-day precipitation totals is proposed in the paper. It utilizes regionally downscaled scenarios of the long-term monthly means of the air temperature, specific air humidity and precipitation projected for Central Slovakia by two regional (RCM) and two global circulation models (GCM). A simplified physically-based model for the calculation of short-term precipitation totals over the course of changing air temperatures, which is used to drive a conceptual rainfall-runoff model, was proposed. In the paper a case study of this approach in the upper Hron river basin in Central Slovakia is presented. From the 1981–2010 period, 20 events of the basin's most extreme average of 5-day precipitation totals were selected. Only events with continual precipitation during 5 days were considered. These 5-day precipitation totals were modified according to the RCM and GCM-based scenarios for the future time horizons of 2025, 2050 and 2075. For modelling runoff under changed 5-day precipitation totals, a conceptual rainfall-runoff model developed at the Slovak University of Technology was used. Changes in extreme mean daily discharges due to climate change were compared with the original flood events and discussed.

Key words: Extreme 5-day precipitation totals, climate change scenarios, rainfall-runoff modelling, extreme floods

1. Introduction

The incidence of several extreme floods in Slovakia over the past decade (*Šťastný and Majerčáková, 2003*) has led to concerns about increases in the frequency and intensity of extreme precipitation in relation to increases in

doi: 10.1515/congeo-2015-0019

the atmospheric water vapour content due to global warming. In Slovakia, extreme daily precipitation totals from the 1950–2000 period were analysed by *Gaál et al. (2004)* at 557 stations, and new design values of K-day (K = 1 to 5 days) precipitation totals for the Slovak territory were developed. Maps of annual maximum K-day precipitation totals with return periods of 50 and 100 years for Slovakia were prepared that indicate a serious risk of high precipitation totals.

The analysis also showed that the dependence of maximum daily precipitation totals on altitudes was insignificant. Nevertheless, the mountainous areas exhibit more cases of daily precipitation totals above 100 mm than do the lowland areas. For estimating future flood risks in mountainous regions, a simplified physically-based model for the calculation of short-term precipitation totals at changing air temperatures and humidity was proposed, which has been used to drive a conceptual rainfall-runoff model (*Lapin and Hlavčová, 2003*). Possible changes in the potential evapotranspiration regime since 1951 and scenarios up to 2100 have been studied by *Lapin et al. (2014, 2015)*. This approach has been used in the upper Hron river catchment in Central Slovakia, where extreme daily precipitation events with durations of 5 days as representative of the flash flood regime have been selected and analysed.

2. Methods

2.1 Climate scenarios of changes in extreme precipitation events

The latest outputs of GCM and RCM scenarios present daily and monthly values of mean, maximum and minimum air temperatures, the variability of precipitation, air humidity, and air pressure. Precipitation and some other elements are mostly dependent on air temperature, air humidity and atmospheric circulation conditions. Scenarios of changes in selected climatic elements in Slovakia have been prepared using model outputs from the Canadian Global General Circulation Model (GCM) called CGCM3.1 and the SRES-B1 (optimistic) and SRES-A2 (pessimistic) emission scenarios, issued in 2011, and the KNMI (Dutch) and MPI (German) Regional Circulation Models, both of which are based on the German ECHAM5

GCM boundary conditions and the SRES-A1B (moderate) emission scenario, issued in 2011 (*Lapin et al., 2012*). All the models are coupled, namely atmosphere-ocean circulation models with greenhouse gasses and aerosols that influence changes in radiative forcing. The results and scenarios of these models are comparable with previous ones based on GCM_S, CGCM1, CCM2, GISS98 and others applied in Slovakia. Analyses of the changes in runoff regimes based on these older scenarios have been published, as in *Hlavčová et al. (1999); Majerčáková (2000); Kostka and Holko (2001); Pekárová and Miklánek (2001); Petrovič (2000).* Teleconnections of inter-annual streamflow fluctuation in Slovakia with Arctic and North Atlantic Oscillations have been studied by *Pekárová and Pekár (2007).*

Based on a regional downscaling of the above models, scenarios of the long-term monthly means of air temperature, water vapour pressure and precipitation have been projected for Central Slovakia (only the 2075 time horizon is shown in Table 1 (*Lapin et al., 2012; 2014*).

In the case of the 1981–2010 base period (Table 1), the values of the dT, qe and qR scenarios are only slightly different for the air temperature (in the convective April-November season, the dT is lower by about 0.7°C using the CGCM3.1 GCM and by about 0.1°C using the KNMI and MPI RCMs). The scenarios of the water vapour pressure and precipitation totals are nearly the same (the deviations are mostly below 5 %).

A simplified equation for calculating short-term precipitation totals at changing air temperature (T) was developed by Lapin (*Lapin and Melo, 2004*):

$$R = g^{-1} \int_{t_0}^{t} \int_{p_c}^{0} \omega \, \frac{\mathrm{d}s}{\mathrm{d}p} \, \mathrm{d}p \, \mathrm{d}t \,, \tag{1}$$

where $g = 9.81\,\mathrm{m\,s^{-2}}$, $\omega = \mathrm{d}p/\mathrm{d}t = -\rho g \boldsymbol{w}$ – e.g., generalized vertical velocity, $\boldsymbol{w}$ – vertical component of the wind velocity vector, s – specific air humidity above the condensation level p_c, p – air pressure, t – time, ρ – air density. For the water vapour partial pressure ($\boldsymbol{e}$) and specific humidity ($\boldsymbol{s}$), a relation exists:

$$\boldsymbol{s} = 0.622\,\boldsymbol{e}/(p - 0.378\,\boldsymbol{e})\,. \tag{2}$$

Table 1. Deviations in the mean monthly air temperature changes (dT) and quotients of the mean monthly water vapour pressure (qe) and precipitation total (qR) changes according to scenarios based on the CGCM3.1-B1, CGCM3.1-A2, KNMI-A1B and MPI-A1B outputs for the centre of Slovakia in the 2075 time horizon compared to the 1951–1980 means (top table) and 1981–2010 means (bottom table).

Model	Element	I	II	III	IV	V	VI	VII	VIII	IX	X	XI	XII
CGCM3.1-B1	dT[°C]	3.45	3.66	3.51	3.08	2.66	2.02	0.94	1.57	2.39	2.53	2.23	2.34
CGCM3.1-B1	qe	1.30	1.30	1.35	1.26	1.16	1.14	1.12	1.11	1.17	1.16	1.18	1.22
CGCM3.1-B1	qR	1.36	0.99	1.38	1.42	1.14	1.16	1.12	1.04	1.02	0.88	1.42	1.15
CGCM3.1-A2	dT[°C]	4.56	4.75	5.06	4.82	3.67	2.87	2.07	3.38	3.76	3.58	3.73	3.14
CGCM3.1-A2	qe	1.43	1.43	1.51	1.41	1.23	1.20	1.18	1.21	1.22	1.22	1.32	1.29
CGCM3.1-A2	qR	1.39	1.10	1.34	1.50	1.21	1.15	0.94	0.87	0.86	1.06	1.34	1.32
KNMI-A1B	dT[°C]	2.81	2.75	2.70	2.17	2.41	3.16	3.17	3.10	2.88	3.06	2.05	2.48
KNMI-A1B	qe	1.25	1.24	1.22	1.15	1.13	1.17	1.13	1.16	1.17	1.21	1.14	1.21
KNMI-A1B	qR	1.24	1.27	1.32	1.16	0.93	0.81	0.65	0.94	1.07	1.04	1.23	1.21
MPI-A1B	dT[°C]	3.11	2.69	2.38	1.90	1.54	2.50	2.37	3.36	3.40	3.34	2.31	2.95
MPI-A1B	qe	1.23	1.21	1.18	1.17	1.14	1.16	1.15	1.17	1.19	1.21	1.15	1.20
MPI-A1B	qR	1.20	1.37	1.24	1.25	0.93	0.92	0.72	0.83	1.16	1.22	1.17	1.31

Model	Element	I	II	III	IV	V	VI	VII	VIII	IX	X	XI	XII
CGCM3.1-B1	dT[°C]	2.12	2.31	1.67	2.19	1.20	0.95	0.55	1.44	1.90	1.90	1.15	2.10
CGCM3.1-B1	qe	1.19	1.18	1.19	1.19	1.08	1.10	1.07	1.09	1.13	1.14	1.08	1.17
CGCM3.1-B1	qR	1.30	1.28	1.41	1.28	1.21	1.23	1.07	0.85	1.07	0.91	1.23	1.17
CGCM3.1-A2	dT[°C]	2.58	3.13	2.86	3.96	2.42	1.58	1.93	3.34	3.35	2.78	2.77	2.75
CGCM3.1-A2	qe	1.27	1.30	1.30	1.34	1.17	1.14	1.15	1.18	1.19	1.18	1.25	1.25
CGCM3.1-A2	qR	1.33	1.44	1.37	1.28	1.23	1.11	0.90	0.74	0.81	1.04	1.26	1.26
KNMI-A1B	dT[°C]	2.11	3.00	2.19	1.75	2.46	3.11	3.25	2.98	2.22	2.70	2.75	2.68
KNMI-A1B	qe	1.20	1.26	1.17	1.12	1.13	1.15	1.14	1.17	1.15	1.20	1.20	1.23
KNMI-A1B	qR	1.17	1.29	1.29	1.15	0.85	0.73	0.73	1.07	1.26	1.24	1.04	1.24
MPI-A1B	dT[°C]	2.66	3.21	1.83	1.25	1.90	2.47	2.54	3.36	2.68	2.70	2.88	2.57
MPI-A1B	qe	1.20	1.22	1.16	1.15	1.14	1.15	1.16	1.18	1.18	1.22	1.21	1.20
MPI-A1B	qR	1.11	1.37	1.33	1.24	0.79	1.00	0.87	1.06	1.38	1.28	1.14	1.20

The dependence of the saturated $\boldsymbol{s}$ ($\boldsymbol{s}^*$) on $\boldsymbol{T}$ at the 900 hPa level is shown in Fig. 2. It is assumed that all the water falls immediately after condensation as precipitation on the Earth's surface. The decrease in $\boldsymbol{s}^*$ at a vertical air motion is in accordance with the adiabatic process for saturated air. In the case of the rising $\boldsymbol{s}^*$ (at a higher $\boldsymbol{T}$), $\boldsymbol{w}$ is also generally increasing, but it depends on the vertical temperature gradient and the vertical thermal instability. Assuming an increase in the turbulent exchange of air humidity and energy at a higher $\boldsymbol{T}$ by 3–4°C in saturated air, the condensation process (and precipitation totals as well) can increase by another 10–50 % in

the summer season. The final calculation of the short-term extreme precipitation totals is based on the expected development of the monthly $\boldsymbol{T}$ and $\boldsymbol{s}$ averages in the 2025, 2050 and 2075 time frames. For example, at a mean of $\boldsymbol{w} = 0.1\,\mathrm{m\,s^{-1}}$, the 24 h precipitation is 35.5 mm for saturated $\boldsymbol{s}^* = 4\,\mathrm{g\,kg^{-1}}$ and 174.5 mm for $\boldsymbol{s}^* = 20\,\mathrm{g\,kg^{-1}}$ at the 900 hPa level. A graphic expression of this simple precipitation eq. (1) is shown in Fig. 1 for a 30-minute duration of stronger rain at a mean vertical velocity of air $\boldsymbol{w} = 1.0\,\mathrm{m\,s^{-1}}$, $\boldsymbol{w} = 2.0\,\mathrm{m\,s^{-1}}$ and $\boldsymbol{w} = 4.0\,\mathrm{m\,s^{-1}}$.

On the basis of this algorithm 5-day precipitation scenarios (Table 2) can be approximately designed. They follow the $\boldsymbol{T}$ and $\boldsymbol{s}$ outputs of the CGCM3.1, the KNMI and MPI-based scenarios do not assume that the $\boldsymbol{w}$ at the condensation process will slightly increase with rising $\boldsymbol{T}$ and $\boldsymbol{s}$ (also, the atmospheric turbulence increases precipitation totals, mainly in the summer months). The dependence of $\boldsymbol{s}^*$ on $\boldsymbol{T}$ is shown in Fig. 2. The projected increase in precipitation totals for extreme precipitation events is up to 20 % higher for the short-term (stormy) totals and up to 10 % higher

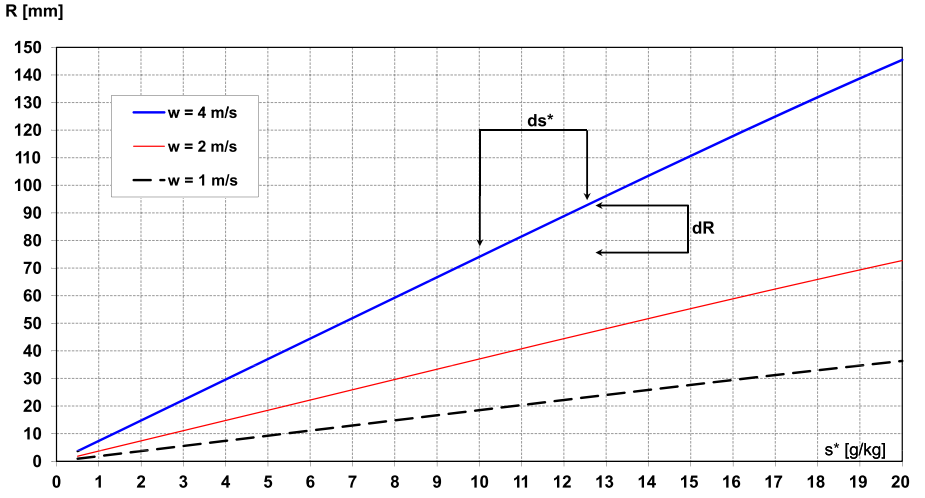

Fig. 1. Dependence of 30-minute precipitation totals (R) on specific humidity s^* at the 900 hPa level (considered as a condensation elevation) and on mean vertical velocity (w); the values of ds^* and dR show an increase in air temperature of 4°C. The contributions of increased w due to rising air temperatures and increased turbulence have to be taken into account (about +30 %).

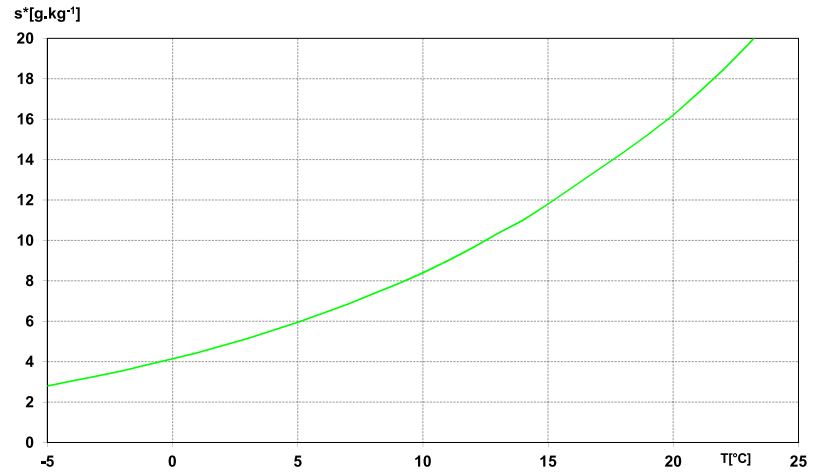

Fig. 2. Dependence of specific humidity s^* on T at 900 hPa level used in Eq. (1).

for 3 to 5-day totals compared to Table 2 (also depending on the intensity of the turbulence). All the data in Table 2 are presented for events with no changes in the vertical velocity ($\boldsymbol{w}$) in the 2075 time horizon and the April to November season.

The values presented in Table 2 can be increased by quotients from 1.10 to 1.20 due to turbulence and increases in vertical velocity w at higher temperatures in the convective season of the year. The average quotients are 1.10 in case of 5-day totals for all the months from IV to XI. For the 1-day and shorter extreme totals are of 1.10 in IV, X and XI, 1.20 in VI, VII and VIII, and 1.15 in V and IX are seen as optimal. These quotients can also be used for comparisons with the 1961–1990 base period. In the case of the 1981–2010 base period, the quotients in the Table 2 are lower because of the higher mean temperatures in 1981–2010 than those in 1951–1980.

In the following part of the study, 20 events of the most extreme basin averages of 5-day precipitation totals in the Hron river basin were selected from the period of 1981–2010. Only events with continual precipitation over 5 days were considered. The daily precipitation totals during the selected extreme events were modified according to the assumed changes in the extreme 5-day precipitation totals for the 4 climate scenarios and the time horizons of 2025, 2050 and 2075 (Table 2). Based on an assumption

Table 2. Quotients of changes in extreme 5-day precipitation totals for the GCM and RCM climate change scenarios and the horizons of the 2025, 2050 and 2075 time frames compared to the 1951–1980 events (top table) and the 1981–2010 ones (bottom table).

Model	Horizon	I	II	III	IV	V	VI	VII	VIII	IX	X	XI	XII
CGCM3.1-B1	2025	1.21	1.28	1.23	1.15	1.17	1.11	1.05	1.05	1.11	1.10	1.13	1.08
	2050	1.27	1.32	1.29	1.20	1.19	1.13	1.05	1.09	1.14	1.14	1.19	1.15
	2075	1.33	1.35	1.30	1.24	1.20	1.14	1.06	1.11	1.17	1.19	1.16	1.21
CGCM3.1-A2	2025	1.27	1.28	1.27	1.15	1.13	1.16	1.05	1.07	1.14	1.12	1.06	1.06
	2050	1.30	1.31	1.34	1.25	1.21	1.15	1.09	1.16	1.19	1.18	1.15	1.14
	2075	1.46	1.48	1.45	1.40	1.28	1.21	1.15	1.25	1.28	1.28	1.29	1.29
KNMI-A1B	2025	1.06	1.09	1.10	1.07	1.05	1.07	1.05	1.06	1.08	1.12	1.01	0.99
	2050	1.14	1.22	1.17	1.12	1.11	1.14	1.11	1.15	1.14	1.17	1.06	1.11
	2075	1.26	1.26	1.23	1.16	1.18	1.23	1.23	1.22	1.21	1.23	1.15	1.23
MPI-A1B	2025	1.05	1.05	1.09	1.07	1.02	1.05	1.04	1.07	1.09	1.14	1.03	1.06
	2050	1.17	1.20	1.16	1.11	1.06	1.10	1.09	1.16	1.16	1.20	1.09	1.16
	2075	1.29	1.25	1.22	1.14	1.11	1.18	1.17	1.24	1.25	1.26	1.17	1.27

Model	Horizon	I	II	III	IV	V	VI	VII	VIII	IX	X	XI	XII
CGCM3.1-B1	2025	1.08	1.15	1.07	1.08	1.06	1.04	1.02	1.04	1.07	1.05	1.05	1.06
	2050	1.14	1.18	1.13	1.13	1.08	1.06	1.03	1.08	1.10	1.09	1.10	1.13
	2075	1.19	1.21	1.15	1.17	1.08	1.07	1.04	1.10	1.14	1.14	1.08	1.19
CGCM3.1-A2	2025	1.07	1.12	1.08	1.09	1.04	1.06	1.04	1.06	1.11	1.06	1.00	1.03
	2050	1.11	1.15	1.15	1.18	1.11	1.06	1.08	1.16	1.16	1.12	1.07	1.10
	2075	1.24	1.30	1.24	1.32	1.18	1.11	1.13	1.24	1.25	1.21	1.21	1.25
KNMI-A1B	2025	1.00	1.11	1.06	1.04	1.05	1.07	1.05	1.05	1.03	1.09	1.05	1.00
	2050	1.08	1.24	1.12	1.08	1.12	1.14	1.12	1.14	1.09	1.15	1.12	1.13
	2075	1.19	1.28	1.20	1.13	1.18	1.23	1.24	1.21	1.16	1.20	1.21	1.25
MPI-A1B	2025	1.01	1.10	1.04	1.03	1.05	1.05	1.05	1.07	1.04	1.09	1.06	1.02
	2050	1.13	1.26	1.11	1.06	1.09	1.10	1.10	1.16	1.10	1.15	1.14	1.13
	2075	1.25	1.31	1.16	1.09	1.14	1.18	1.18	1.24	1.20	1.20	1.22	1.24

of dry periods between extreme precipitation events in the future, other daily precipitation totals in the original data set were changed according to the climate change scenarios (Table 1 for T and R, Table 3 for potential evapotranspiration E_0). The air temperature, precipitation totals and potential evapotranspiration were modified for the whole period of 1981–2010 according to the climate scenarios in a monthly time step for each day. The changes (increases were positive, decreases were negative) in potential evapotranspiration [%/month] in comparison with the reference period of 1951–1980 or 1981–2010 according to the 4 GCMs/RCMs and the Zubenok method are illustrated in Table 3 (*Lapin et al., 2014*).

In case of the 1981–2010 period the quotients are about 0 % to 2 % lower

Table 3. Changes in potential evapotranspiration dE_0 [%] for the GCM (CGCM3.1-B1 and A2) and RCM (KNMI and MPI) climate change scenarios and the horizons of 2025, 2050 and 2075 compared to 1951–1980 (top table), and 1981–2010 base period (bottom table).

Model	Horizon	I	II	III	IV	V	VI	VII	VIII	IX	X	XI	XII
CGCM3.1-B1	2025	7.8	14.5	6.4	5.1	10.4	6.5	0.3	0.9	5.4	14.7	4.5	−2.3
	2050	8.5	16.6	4.9	8.8	11.2	5.3	−0.9	2.3	8.2	16.9	6.4	−1.2
	2075	6.7	16.6	0.9	11.6	11.2	4.9	−2.4	3.4	8.0	20.6	5.4	1.8
CGCM3.1-A2	2025	10.9	14.1	6.8	6.3	9.6	8.1	0.0	3.5	13.0	19.0	4.3	−2.0
	2050	7.9	12.9	6.3	11.0	11.9	5.9	1.1	10.4	13.6	22.3	9.2	−2.0
	2075	7.6	16.4	6.2	19.3	14.6	7.0	2.1	11.8	21.7	30.5	14.7	3.8
KNMI-A1B	2025	1.7	3.5	8.9	6.4	6.0	3.7	3.7	4.3	7.6	11.1	7.7	2.6
	2050	5.9	8.8	13.3	7.5	7.9	5.8	7.6	9.9	14.7	16.8	10.8	5.9
	2075	9.1	9.5	13.6	9.9	12.2	12.0	15.6	16.2	19.6	19.2	14.1	5.9
MPI-A1B	2025	7.1	−0.3	11.9	7.3	0.1	2.1	2.1	6.5	9.1	24.0	17.3	12.0
	2050	18.0	15.1	17.3	3.9	1.3	3.2	3.4	11.7	13.6	29.0	23.5	25.9
	2075	21.8	15.2	13.5	2.5	2.5	7.3	7.2	17.6	24.5	31.2	21.0	34.6

Model	Horizon	I	II	III	IV	V	VI	VII	VIII	IX	X	XI	XII
CGCM3.1-B1	2025	2.2	9.0	2.6	2.4	2.7	1.1	0.7	1.8	5.8	2.9	4.3	3.6
	2050	2.8	11.0	1.2	6.0	3.5	0.0	−0.6	3.2	8.7	4.9	6.2	4.9
	2075	1.1	11.0	−2.6	8.7	3.4	−0.4	−2.1	4.3	8.5	8.2	5.2	7.9
CGCM3.1-A2	2025	1.8	5.7	2.5	3.8	3.3	2.3	0.9	6.2	13.1	7.4	0.5	0.6
	2050	−1.0	4.6	2.0	8.4	5.5	0.2	2.1	13.3	13.7	10.4	5.3	0.6
	2075	−1.3	7.8	1.9	16.6	8.1	1.2	3.1	14.7	21.9	17.8	10.6	6.5
KNMI-A1B	2025	1.3	3.7	6.5	3.8	5.9	3.5	3.3	3.3	1.1	3.0	4.8	1.6
	2050	5.4	9.0	10.8	4.8	7.8	5.6	7.3	8.8	7.7	8.4	7.8	4.9
	2075	8.6	9.7	11.1	7.2	12.1	11.8	15.2	15.0	12.3	10.6	11.0	4.8
MPI-A1B	2025	6.2	10.3	1.9	2.7	2.7	1.8	2.3	5.6	−0.3	2.3	7.7	−4.6
	2050	16.9	27.5	6.9	−0.6	4.0	2.9	3.6	10.7	3.8	6.5	13.3	7.2
	2075	20.7	27.6	3.4	−1.9	5.2	6.9	7.5	16.5	13.8	8.3	11.1	14.7

because of different input data in 1981–2010 compared those in 1951–1980 (Table 3). The values of E_0 has been calculated by the Zubenok method depending on the saturation deficit obtained from daily data and different monthly equations during the year and in selected geobotanic regions.

2.2 Rainfall-runoff model for modelling extreme floods

The HRON rainfall-runoff model used in the presented study for the simulation of catchment runoff belongs to a group of conceptual lumped models. It primarily works in a daily time step and has been built on the basis of

the Swedish HBV model (*Bergström, 1976*) by following its main structure. The different components of the hydrological cycle are represented by two reservoirs within the HRON model: 1) the upper reservoir used to simulate fast surface runoff and hypodermic flow, and 2) the lower reservoir acting as a storage space for underground water which simulates the base flow. The model is further divided into three separate modules, which are represented by snow, soil, and flow routing modules. The snow module simulates the process of the accumulation and melt of snow cover using a simple concept of threshold temperatures and a degree-day melting approach (*Golledge and Levy, 2001*). The module utilizes three threshold temperature parameters, where the first two partition the mean daily precipitation into rain (tempRain) and snow (tempSnow), based on a ratio calculated using the rain and snow temperature threshold parameters. The third temperature threshold determines the melting temperature (tempMelt) of snow accumulated in the catchment. Snow melt starts at air temperatures higher than tempSnow and is proportional to the degree day factor (DDF) and the difference between the actual and tempSnow temperature. The last parameter of the snow module (SCF) corrects the difference between the real and measured amount of snow, which arises from the inaccuracy of rainfall gauges during snowfall events.

The soil module represents the hydrological processes taking place under the soil surface. It simulates the process of the generation of individual runoff components and changes in the state of the catchment. The saturation of the catchment with water is given by the amount of water stored in the three fictive reservoirs. The first represents the amount of water stored in the upper soil layers (soil moisture) and is driven by three model parameters: the maximum soil moisture storage (FC), the soil moisture state, above which the evaporation occurs at its potential rate (LPE), and a parameter (RC) determining the amount of water contributing to the upper reservoir store.

In the third module all the runoff components are simulated in the upper and lower reservoirs. The upper reservoir is fed with the excess rainfall and water seeping from the soil moisture store. In this reservoir overland and hypodermic flows are simulated through very fast (K0) and fast (K1) storage coefficients, while the overland flow only occurs when the amount of water stored in the upper reservoir is higher than the threshold (UZL).

The lower reservoir is fed with water percolating from the upper reservoir at a constant rate given by a parameter (PERC). It simulates the base flow using a slow storage coefficient (K2). The routing module transforms all the flow components from both reservoirs using a triangular function described by a parameter (MAXBAS). The 14 free parameters (*Valent et al., 2012*) were estimated in the automatic calibration process described in the next section (Table 4).

Table 4. HRON rainfall-runoff model parameters together with their bounds.

Parameter	Description and units	Range
Fc	*field capacity* – represents the maximum amount of water that the upper part of the soil can hold [mm]	150 – 300
Rc	coefficient influencing the amount of water contributing to the soil moisture and the upper reservoir [–]	1 – 3
uzl	*upper zone limit* – threshold value determining the occurrence of surface runoff q0 [mm]	10 – 40
tempRain	threshold temperature above which the entire precipitation is liquid [°C]	1 – 7
tempMelt	threshold temperature determining the start of the snow melting [°C]	−3 – 1.5
tempSnow	threshold temperature under which the entire precipitation is solid [°C]	−7 – (−2)
ddf	*degree-day factor* – determines the speed of the snow melting [mm]	0.5–3
perc	*percolation* – the amount of water percolating from the upper to the bottom reservoir [mm]	0.5 – 4
Lpe	*limit of potential evapotranspiration* – used to estimate the potential evapotranspiration [–]	0.5 – 1
k0 k1 k2	empirical parameters influencing the surface (q0), subsurface (q1) and base (q2) flows [–]	1 – 15 1 – 20 10 – 60
Scf	*snow correction factor* – corrects the measured snow precipitation [–]	0.8 – 1.5
Maxbas	parameter determining the amount of days into which the catchment runoff is divided	1 – 4

The rainfall-runoff model presented in the study is used for the continuous and subsequent event-based simulation of the catchment runoff in a daily time step. In the first case the model is used to simulate the catch-

ment runoff from the whole period in order to obtain a better idea of the amount of water stored in the catchment. In the second case the model is only used as an event-based model to simulate runoff induced by the selected 5-day rainfall events. In this case the results from the continuous simulation are used to adjust the antecedent conditions in the catchment. This task requires that the model perform equally well on low and high flows. In order to do so, a new 2-regime modelling scheme was proposed. In this scheme different sets of parameters were used to simulate low and high flows respectively. The decision as to which regime (the set of parameters) is used to simulate the flow on day i depends on the value of the flow from the previous day $i-1$.

2.3 Calibration of the model and efficiency measures

The calibration of the 2-regime rainfall-runoff model used was divided into three steps. In the first step the parameters used to simulate low and medium flows were estimated using an automatic calibration procedure that utilizes a harmony search algorithm (see e.g. *Geem et al., 2001*). In this case a split-sample calibration procedure (see *Klemeš, 1986*) was used where the observed time period was split into two halves (1981–1995 and 1996–2010). Each half was then used for the model's calibration, while the second half was used for its validation. The best parameter set was selected based on the value of the Nash-Sutcliffe efficiency criterion (NSE), which was used as an optimization function (*Nash and Sutcliffe, 1970*).

$$NS = 1 - \frac{\sum_{i=1}^{n} \left(Q_{sim,i} - Q_{obs,i}\right)^2}{\sum_{i=1}^{n} \left(Q_{sim,i} - \overline{Q}_{obs}\right)^2} \tag{3}$$

In the second step of the 2-regime model's calibration, the parameters used to simulate high flows were estimated. In this case the optimization algorithm minimized the sum of the squares of the residuals (SSR), which was only calculated for the largest flood events selected.

$$SSR = \sum_{i=1}^{n} \left(Q_{sim,i} - Q_{obs,i}\right)^2 \tag{4}$$

The floods were selected from the whole time period using the peaks over threshold (POT) method, when 4 flood events per year were selected on

average (a total of 120 events). In order to simplify the estimation of the beginning and the end of a particular flood event, they were set as ±2 days from their peaks. The last step of the calibration included the estimation of the threshold determining whether the catchment runoff was considered as low or high. This threshold was estimated using a pattern search algorithm (*Hooke and Jeeves, 1961*) with SSR used as an objective function, which was again only calculated for the flood events selected.

In order to account for the model and calibration scheme's uncertainties, 10 independent calibrations were executed (10 for each of the data halves) (see e.g. *Gupta et al., 2005; Valent et al., 2012*).

The model was calibrated 10 times using both the first (1981–1995) and second (1996–2010) halves of the input dataset. The Table 5 shows the NS values calculated for the whole dataset and the SSR calculated for the high flows. For the simulation of runoff in changed climate conditions the set of model parameters obtained from the calibration period 1996–2010 and the iteration number 9 was chosen.

Table 5. The results of the calibration and validation of the two-regime rainfall runoff model.

	Cal. 1981–1995		Val. 1996–2010		Val. 1981–1995		Cal. 1996–2010	
Iteration	NS	SSR	NS	SSR	NS	SSR	NS	SSR
1	0.798	1.57E+05	0.775	2.14E+05	0.817	1.23E+05	0.793	1.17E+05
2	0.795	1.54E+05	0.774	2.20E+05	0.829	1.19E+05	0.766	1.26E+05
3	0.810	1.62E+05	0.778	2.22E+05	0.833	1.23E+05	0.799	1.22E+05
4	0.791	1.86E+05	0.742	2.62E+05	0.797	1.51E+05	0.784	1.39E+05
5	0.785	1.92E+05	0.742	2.64E+05	0.790	1.58E+05	0.780	1.31E+05
6	0.796	1.78E+05	0.773	2.19E+05	0.827	1.16E+05	0.785	1.35E+05
7	0.803	1.65E+05	0.739	2.69E+05	0.794	1.60E+05	0.787	1.44E+05
8	0.791	1.83E+05	0.737	2.71E+05	0.789	1.60E+05	0.787	1.33E+05
9	0.801	1.50E+05	0.790	1.89E+05	0.812	1.13E+05	0.781	1.20E+05
10	0.790	1.58E+05	0.747	2.62E+05	0.800	1.54E+05	0.753	1.47E+05
Mean	0.796	1.68E+05	0.760	2.39E+05	0.809	1.38E+05	0.782	1.31E+05

An improvement of the model ability to simulate high flows is illustrated in Fig. 3 where hydrographs of an observed flood wave and simulated flood waves by the one- and two-regime model are graphically compared. The improvement is also visible in the comparison of cumulative frequency curves

of observed and simulated maximum mean daily discharges of the selected 120 events (Fig. 4).

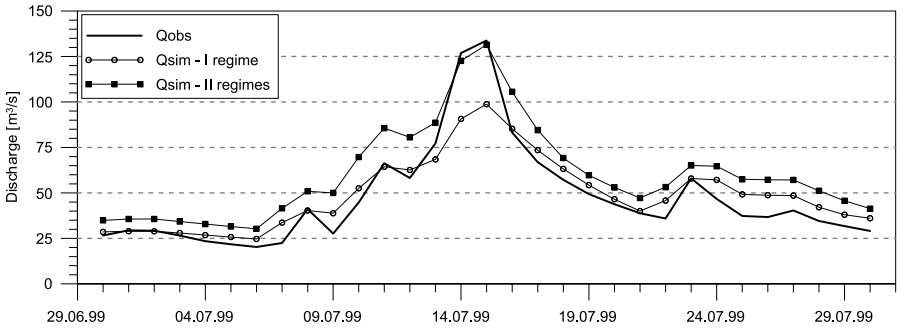

Fig. 3. A comparison between the observed mean daily discharges and simulations using a traditional one-regime model and a two-regime model enabling the separate simulation of the low and high flows.

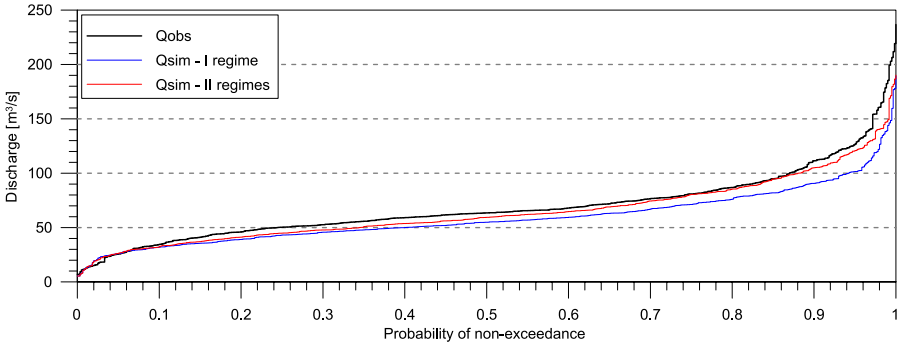

Fig. 4. A comparison of the cumulative frequency curves calculated for the observed and the two simulated flows (blue line for the one-regime model and red line for the two-regime model).

2.4 Short description of the upper Hron river basin

The Hron River is a left-side tributary of the River Danube; its basin is located in Central Slovakia. The catchment is feather-shaped and located along the long main river with its numerous shorter tributaries. The upper part of the basin with its outlet in Banská Bystrica as a representative for

the mountainous regions of Slovakia was selected for this study. The basin has an area of 1766 km^2; the minimum elevation of the basin is 340 m a.s.l.; the maximum elevation is 2004 m a.s.l.; and the mean elevation is 850 m a.s.l. Seventy percent of the basin's area is covered by forest, 10 % by grasslands, 17 % by agricultural land and 3 % by urban areas. The location of the basin within the territory of Slovakia is shown in Fig. 5.

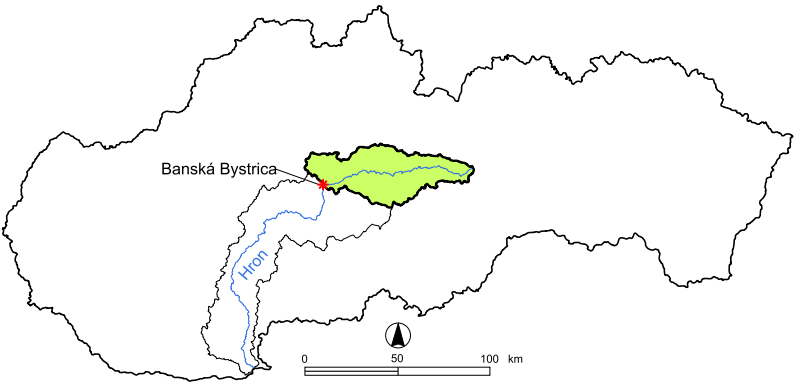

Fig. 5. Location of the Upper Hron River basin in Slovakia.

3. Results

In the following part of the study the impact of climate change-induced extreme precipitation totals on the flood regime in the upper Hron River basin was estimated. First, 20 events of the most extreme basin averages of 5-day precipitation totals were selected from the period of 1981–2010. Only events with continual precipitation over 5 days were considered. The dates of the selected precipitation events, 5-day precipitation totals, maximum and minimum daily precipitation during the events are listed in Table 6.

The continuous and event-based simulations of flood events in changed climate conditions were provided using the calibrated Hron rainfall-runoff model. In the first step the model was used to simulate the catchment runoff continually for the period 1981–2010. The input data to the model (the mean daily air temperatures, daily precipitation totals and daily potential evapotranspiration) were modified for the whole period according to

Table 6. The selection of the 20 largest 5-day precipitation events in the period 1981–2010.

Rank	Beginning		End	5-day precipitation [mm]	Daily maximum [mm]	Daily minimum [mm]
1	06.08.2002	–	10.08.2002	113.2	41.3	2.4
2	16.07.2001	–	20.07.2001	102.5	44.2	3.8
3	10.07.1999	–	14.07.1999	94.0	31.7	5.7
4	27.08.1996	–	31.08.1996	91.4	51.3	3.2
5	13.11.1991	–	17.11.1991	83.7	31.8	0.6
6	13.07.2002	–	17.07.2002	82.8	46.9	2.6
7	10.04.1994	–	14.04.1994	82.7	27.4	2.2
8	21.12.2009	–	25.12.2009	80.6	27.0	3.2
9	09.10.1991	–	13.10.1991	78.6	28.6	3.5
10	20.05.1984	–	24.05.1984	76.0	35.7	2.4
11	13.08.2010	–	17.08.2010	75.6	29.0	0.0
12	03.05.2010	–	07.05.2010	72.5	27.0	5.5
13	23.07.2010	–	27.07.2010	72.1	36.5	0.1
14	10.10.2009	–	14.10.2009	72.0	40.0	1.3
15	31.07.2005	–	04.08.2005	71.6	26.7	0.0
16	17.07.1997	–	21.07.1997	71.5	40.2	2.6
17	08.06.1995	–	12.06.1995	69.7	26.4	2.9
18	23.12.1993	–	27.12.1993	69.4	33.3	3.1
19	29.10.1990	–	02.11.1990	68.7	49.5	0.6
20	28.05.1981	–	01.06.1981	67.0	37.4	2.2

the climate scenarios in a monthly time step for each day (Tables 1 and 3). In the second step the model was only used as an event-based model to simulate runoff induced by the selected 5-day rainfall events. In this case the results from the continuous simulation were used to adjust the antecedent conditions in the catchment. The daily precipitation totals during the selected extreme events were modified according to the assumed changes in the extreme 5-day precipitation totals for the 4 climate scenarios and the time horizons of 2025, 2050 and 2075 (Table 2).

For the changed climate inputs in all of the 20 extreme precipitation events selected, the mean daily discharges using the calibrated rainfall-runoff model were simulated and compared with the original floods. An example of the comparison between the simulated original mean daily discharges and the simulated floods in the future time horizons of 2025, 2050 and 2075 is

shown in Fig. 6.

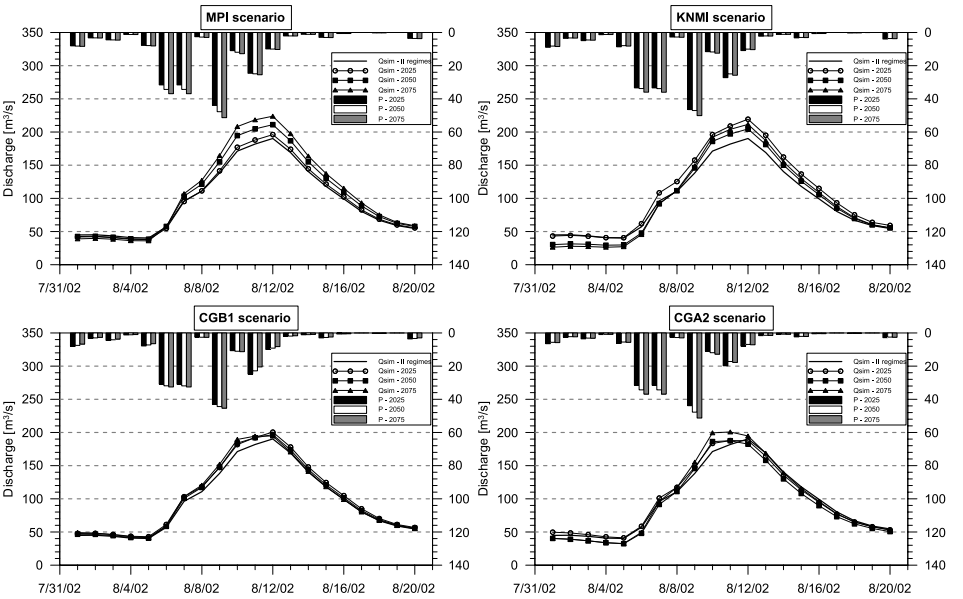

Fig. 6. Comparison between the simulated original mean daily discharges and the simulated a) MPI, b) KNMI, c) CGB1 and d) CGA2 scenario discharges for selected flood events induced by 5-day 6.8.–10.8.2002 rainfall events. The simulations were carried out for the 2025, 2050 and 2075 time horizons.

The changes in mean daily discharges due to changes in extreme precipitation were calculated for each flood induced by one of the 20 highest 5-day rainfall events. Fig. 7 illustrates boxplots showing the relative changes in maximum mean daily discharges of 20 flood events simulated for the various climate scenarios and for three time horizons (2025, 2050, 2075) in comparison with simulated original flood events. The maximum and median of percentual changes are listed in Table 7.

The analysis of changes in extreme events due to climate change can indicate an increase in extreme short-term precipitation and an increase in the floods caused. From the results of all the simulated events, it can be seen that in comparison with the original runoff, the maximum mean daily discharges of the simulated flood waves can increase up to 43–55 % in 2025, up to 94–115 % in 2050, and up to 115–166 % in the 2075 time horizon.

Table 7. The maximum and median of relative changes in the maximum mean daily discharges of 20 flood events simulated for the various climate scenarios and for three time horizons (2025, 2050, 2075) in comparison with simulated original flood events.

Scenario	MPI			KNMI			CGB1			CGA2		
Horizon	2025	2050	2075	2025	2050	2075	2025	2050	2075	2025	2050	2075
Maximum	55	110	158	53	115	165	55	102	124	43	94	166
Median	28	34	49	23	16	29	16	20	33	23	15	28

The median of the changes in the maximum mean daily discharges is in the range of 16–28 % in 2025, 15–24 % in 2050, and 28–49 % in 2075.

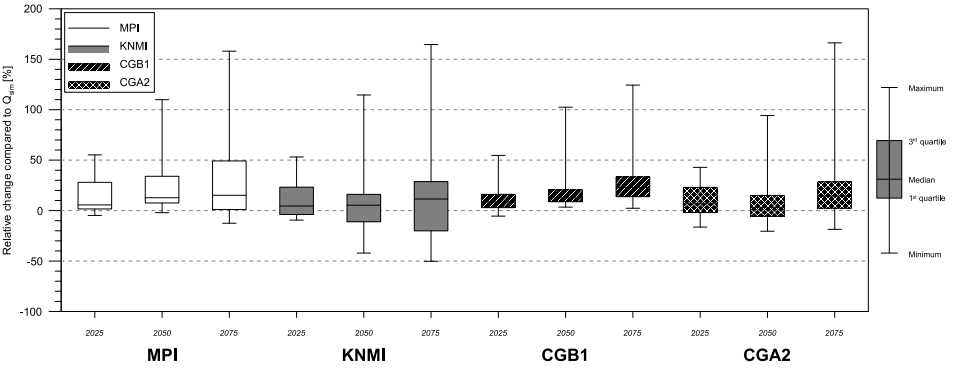

Fig. 7. Boxplots showing the relative changes in the maximum mean daily discharges of 20 flood events simulated for the various climate scenarios and for three time horizons (2025, 2050 and 2075) in comparison with simulated original flood events.

4. Conclusions

It is possible to prepare climate change scenarios such as daily data series and extreme weather events from the modified outputs of the latest regional climate change models (RCMs). This is mainly due to the more detailed topography and better physics of the newest RCMs with a 25×25 km resolution of the grid points. The regional and local modifications (statistical and dynamic downscaling) of the RCM outputs need high-quality measured data during the control period (the 30-year period from 1951–2010) as well

as high-quality hydrological data measured during extreme flood events.

The methodology proposed for the calculation of short-term precipitation totals at changing air temperatures by the simplified physically-based model results in more representative extreme short-term precipitation totals, which are higher in comparison with the direct outputs from GCMs and RCMs. This is mainly influenced by smoothed precipitation totals fields in climatic models due to the horizontal resolution of the grid points (25×25 km to 300×300 km), which does not sufficiently represent actual precipitation conditions during extreme events.

From the analysis of the changes in extreme events due to climate change, an increase in extreme 5-day precipitation totals and floods was indicated. The uncertainties of the methodology used can affect the estimation of the model parameters which were calibrated using the data from the period 1981–2010 and transferred to the future time horizons. Nevertheless, an estimation of the impact of climate change on a flood regime by continuous and event-based simulations of floods using a rainfall-runoff model allows for the inclusion of physically-developed scenarios for changes in 5-day extreme precipitation totals. The results of the simulated changes in extreme floods can be more realistic and provide better assumptions for increases in flood risks in the future.

On the one hand, it is assumed that possible changes in future precipitation regimes can modify extreme floods due to the more frequent occurrence of dry periods prior to significant 5-day precipitation events. On the other hand, extreme precipitation events can be even more significant due to dynamic causes (increases in the atmospheric vertical velocity, better dynamic conditions for thunderstorms and the development of mesocyclones) – see *Fedorovich et al. (2004); Lapin et al. (2012); IPCC (2014).*

Acknowledgments. The research presented in this paper was supported under the APVV-0303-11 and VEGA 1/0776/13 projects. All the support is gratefully acknowledged.

References

Fedorovich E, Rotunno R., Stevens B., Eds, 2004: Atmospheric turbulence and mesoscale meteorology, 2004. Cambridge University Press, 280 pp.

Bergström S., 1976: Development and application of a conceptual runoff model for Scandinavian catchments: Bulletin Series A, Lund Institute of Technology/University of Lund, No. 52, 134 pp.

Gaál L., Lapin M., Faško P., 2004: Several day maximum precipitation totals in Slovakia. In.: Rožnovský J. and Litschmann T. (ed): Extremes of Weather and Climate, Brno, 15 pp.

Geem Z. W., Kim J. H., Loganathan G. V., 2001: A New Heuristic Optimization Algorithm: Harmony Search. Simulation, **70**, 2, 60–68.

Golledge N. R., Levy R. H., 2001: Geometry and dynamics of an East Antarctic Ice Sheet Outlet Glacier, Under Past and Present Climates. J. Geophys. Res., **116**, F03025, doi: 10.1029/2011JF002028.

Gupta H. V., Beven K. J., Wagener T., 2005: Model Calibration and Uncertainty Estimation. In: Anderson M. G. (ed): Encyclopaedia of Hydrological Sciences, Wiley, Chichester, 2015–2031.

Hlavčová K., Szolgay J., Čunderlík J., Parajka J., Lapin M., 1999: Impact of climate change on the hydrological regime of rivers in Slovakia. Publication of the Slovak Committee for Hydrology No. 3. NCH UNESCO, SUT, Bratislava, 101 pp.

Hooke R., Jeeves T. A., 1961: Direct search solution of numerical and statistical problems. Journal of the Association for Computing Machinery (ACM), **8**, 2, 212–229.

IPCC, 2014: Climate change 2013. The physical science basis: Cambridge University Press, 1552 pp., ISBN: 9781107661820, <https://www.ipcc.ch/report/ar5/wg1/>.

Klemeš V., 1986: Operational testing of hydrological simulation models. Hydrological Sciences Journal, **31**, 1, 13–24.

Kostka Z., Holko L., 2001: Vegetation change and hydrological regime of a mountain catchment. Publication of the Slovak National Climate Program, No. 10, SHMI and Slovak Ministry of the Environment, Bratislava, 82–93.

Lapin M., Hlavčová K., 2003: Changes in Summer Type of Flash Floods in the Slovak Carpathians due to Changing Climate. Proceedings of the International Conference on Alpine Meteorology and MAP2003 Meeting, Brig, Switzerland. Publ. of MeteoSwiss, **66**, 105–108.

Lapin M., Melo M., 2004: Methods of climate change scenarios projection in Slovakia and selected results. J. Hydrol. Hydromechan., **52**, 4, 224–238.

Lapin M., Bašták I., Gera M., Hrvoľ J., Kremler M., Melo M., 2012: New climate change scenarios for Slovakia based on global and regional general circulation models. Acta Meteorologica Universitatis Comenianae, **37**, 25–73.

Lapin M., Damborská I., Gera M., Hrvoľ J., Melo M., 2014: Possible changes in evapotranspiration, air humidity and irrigation characteristics in Slovakia. EMS Annual Meeting Abstracts. 11. EMS2014-518-1. 2014. 14th EMS / 10th ECAC Prague.

Lapin M., Damborská I., Gera M., Hrvoľ J., Melo M., 2015: Trends of evapotranspiration in Slovakia, including scenarios up to 2100. International Bioclimatological Conference: Toward Climatic Services. Bioclimatological Society SAS, Nitra, 5 pp.

Majerčáková O., 2000: Hydrological monitoring and modelling of possible monthly runoff change. Publication of the Slovak National Climate Program, No. 9, SHMI and Slovak Ministry of the Environment, Bratislava, 5–14.

Nash J. E., Sutcliffe J. V., 1970: River flow forecasting through conceptual models 1. A discussion of principles. J. Hydrology, **10**, 3, 282–290.

Pekárová P., Miklánek P., 2001: Design discharge changes of the Uh river at Lekárovce station. Acta Hydrologica Slovaca, **2**, 2, 233–240.

Pekárová P., Pekár J., 2007: Teleconnections of inter-annual streamflow fluctuation in Slovakia with Arctic Oscillation, North Atlantic Oscillation, Southern Oscillation, and Quasi-Biennial Oscillation phenomena. Advances in Atmospheric Sciences, **24**, 4, 655–663.

Petrovič P., 2000: Climate change impact on hydrological regime in the Nitra river basin. Publication of the Slovak National Climate Program, no. 9, SHMI and Slovak Ministry of the Environment, Bratislava, 58–73.

Šťastný P., Majerčáková O., 2003: The re-construction of flood occurred at Štrba in July 2001. Acta Hydrologica Slovaca, **4**, 2.

Valent P., Szolgay J., Riverso C., 2012: Assessment of the uncertainties of a conceptual hydrologic model by using artificially generated flows. Slovak Journal of Civil Engineering, **20**, 4, 35–43.